Optimal ride characteristics of wheeled space rovers with trailing arm suspension: A parametric study

Ahmed G. Fathy[1], Mostafa Sh. Asfoor[2] and Ahmed M. Ali[2]

[1] Defense Research Center, Egyptian Armed Forces
[2] Automotive Engineering Department, Military Technical College

E-mail : *ahmed.gaber.mtc@gmail.com*

Abstract. The purpose of this paper is to introduce a systematic approach for improving and optimizing the ride performance in space rovers on wheels. Quarter rover models (QRM) are in use for years to study the static and dynamic behaviour of the rover. The parametric investigation studies the behaviour of steady state response on static and dynamic conditions of road through the influence of multiple rover's characteristics. Some of rover parameters are considered including the trailing arm length, wheel radius, trailing arm angle, wheel rotation angle, damping ratio and torsional spring rate, etc. The analysis of results put forward a key-tuning parameters for improving the ride specifications of space rovers under normal operating conditions.

Keywords: rover dynamics, quarter model, road profile, power spectral dens

1. Introduction

1.1 Background

The suspension system is assumed to be one of the most significant part of the rovers [1]. It is used to reduce the impact loads and effect of irregularity of the road for improving the rover ride comfortability and stability [2]. One of the most effective model to study the comfortability and stability of the rover is QRM suspension mechanism. QRM consists of quartile of the rover (one wheel) for the rovers that consists of four wheels. It can be divided into damper, spring, wheel, knuckle and part of chassis(body). Some parameters are assumed on that model, but that doesn't change the engineering applications using this dynamic model system [3].

1.2 Design of a space Rover suspension system

Needless to say that rovers are one of the most important used vehicles in exploration of solar system planets [4]. Most of the designs of these rovers have been developed to face the surface nature of planets and Moon [5]. During the operations of exploration, a very long distances must be reached in short period due to the obstacles that the explorers face like different climate, environment and the communications[6, 7]. For the rover, different designs for suspension system of rovers have been suggested on rough terrain [8]. Although some of these different mechanisms have used in mobile robotics. The space rover (GURA) is one of space rovers that consists of six wheels with six trailing arms that working individually [9, 10]. In this research, using a quarter rover model mechanism, kinematic, kinetics and equations that represents its motion, the parameters will be tuned to make the performance more suitable for the space rover suspension [11].

Figure 1. GURA Space Rover [12].

1.3 Dynamics of QRM

Rover models are divided into three categories: full-rover-model [13], half-rover-model [14] and quarter-rover- model. Quarter rover model system is a system of two independent coordinates [15], which divided into two bodies: Sprung and unsprung masses as follows (rover body) ,(suspension, wheel, tire). QRM is a simple model where stiffness and damping are used of the system so that it cannot be considered that everything is rigid (which is not representative in a physical model). So that the stiffness and damping of the respective tire and wheel are considered between the suspension and the road, the stiffness and damping of the respective spring and damper are also considered between the rover body and the suspension components.

1.4 Working principle of QRM

The core principle of QRM suspension mechanism is to reduce and eliminate the mechanical energy by dissipating it as a heat in shock absorbers [16, 17]. It reserves a respective motion between the wheels and the body (chassis) by reducing the force transmitted from the wheel to the body(chassis). The suspension mechanism works to make the ride more comfortable and safe for the users [18]. In riding conditions when the wheel moves over a bump or irregular terrain the impact force coming from the wheel to spring makes it compresses storing this force and then the spring expands, the damper works to absorb the vibration and reduce it until it ceased.

2. Modelling of ride specifications of space rover

Essential modelling parameters of QRM are required to be defined in advance is given in table 1.

2. 1 Mathematical representation of simplified QRM:
QRM divided to the chassis (rover body), a trailing arm that is connected to the knuckle and the wheel. This replica shows a quarter rover that affected by a hydro pulse actuator [20].
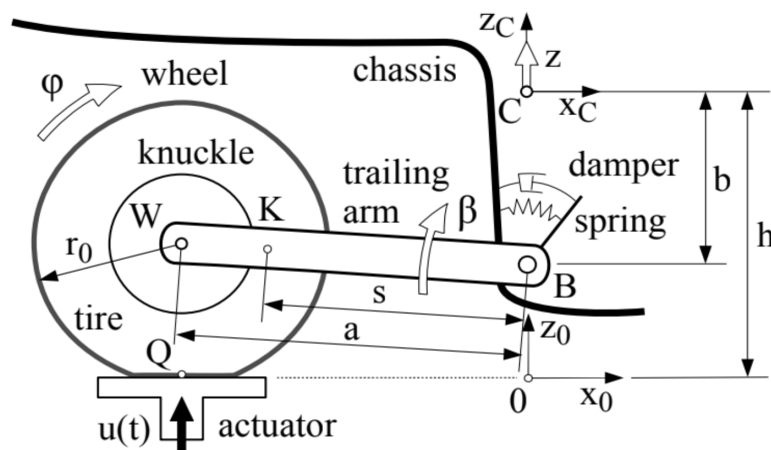
Figure 2. Simplified QRM (coordinates and dimensions).

Table 1. QRM parameters needed for modelling the system [19].

Symbol	Value	Unit	Meaning
g	9.810	$[m/s^2]$	Gravity
s	0.250	$[m]$	Distance from joint B to trailing arm centre
a	0.400	$[m]$	Distance from joint B to wheel centre
b	0.310	$[m]$	Distance from chassis centre to joint B
h	0.600	$[m]$	Height of chassis centre
r_o	0.305	$[m]$	Tire radius
m_C	200	$[kg]$	Corresponding chassis mass
m_K	35	$[kg]$	Knuckle(trailing arm) mass
m_W	15	$[kg]$	Wheel mass (rim and tire)
θ_K	0.6	$[kg.m^2]$	Inertia of knuckle(trailing arm)
θ_W	0.8	$[kg.m^2]$	Inertia of wheel
T_s^0	1200	$[N.m]$	Preload in torsional spring
c_s	10000	$[N.m/rad]$	Torsional spring rate
d_s	800	$[N.m.s]$	Damping coefficient.
c_x	180000	$[N/m]$	Longitudinal tire stiffness
c_z	220000	$[N/m]$	Vertical tire stiffness
d_x	150	$[N.s/m]$	Longitudinal tire damping
Ω	---------	$[rad/m]$	Wave number
Φ_0	$1 \times 10^{-\times}$	$[m^2/(rad/m)]$	Power spectral density
ω	2	$unitless$	Waviness
Ψ	--------	rad	Phase lag between the left and right tracks
μ	1	$unitless$	Friction coefficient
v	22.222	$[m/s]$	Vehicle velocity

Kinematics of QRM:

The QRM can be divided into three rigid bodies (chassis, wheel, knuckle). the alignment of these rigid bodies are coordinated by three generalized coordinates $(z, \beta, \emptyset)$ for respective position ,velocity, and acceleration of the chassis centre c [21]. the position, velocity and acceleration of knuckle and wheel are simply defined by:

Kinematics relations for knuckle centre (k c):
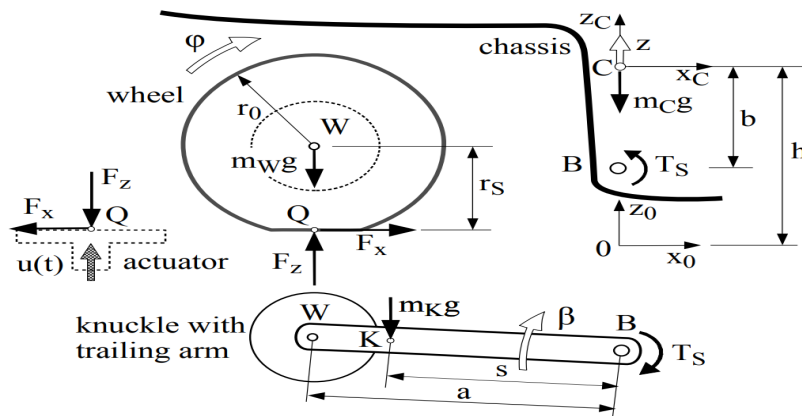
The knuckle position vector with respect to centre c:

$$r0 = \begin{bmatrix} 0 \\ 0 \\ h+z \end{bmatrix} + \begin{bmatrix} 0 \\ 0 \\ -b \end{bmatrix} + \begin{bmatrix} -s\,cos\beta \\ 0 \\ s\,sin\beta \end{bmatrix}$$

(1)

The velocity vector could be determined by taking derivative of equation (1) with respect to time:

$$v0 = \begin{bmatrix} 0 \\ 0 \\ 1 \end{bmatrix} \dot{z} + \begin{bmatrix} s\,sin\beta \\ 0 \\ s\,cos\beta \end{bmatrix} \dot{\beta}$$

(2)

The acceleration vector is determined by taking derivative of equation (2) with respect to time:

$$a0 = \begin{bmatrix} 0 \\ 0 \\ 1 \end{bmatrix} \ddot{Z} + \begin{bmatrix} s\,sin\beta \\ 0 \\ s\,cos\beta \end{bmatrix} \ddot{\beta} + \begin{bmatrix} s\,cos\beta \\ 0 \\ -s\,sin\beta \end{bmatrix} \dot{\beta}^2$$

(3)

Kinematics relations for wheel centre (w c):

The wheel position vector with respect to centre c:

$$r0 = \begin{bmatrix} 0 \\ 0 \\ h+z \end{bmatrix} + \begin{bmatrix} 0 \\ 0 \\ -b \end{bmatrix} + \begin{bmatrix} -a\ cos\beta \\ 0 \\ a\ sin\beta \end{bmatrix} \tag{4}$$

The velocity vector could be determined by taking derivative of equation (4) with respect to time:

$$v0 = \begin{bmatrix} 0 \\ 0 \\ 1 \end{bmatrix} \dot{z} + \begin{bmatrix} a\ sin\beta \\ 0 \\ a\ cos\beta \end{bmatrix} \dot{\beta} \tag{5}$$

The acceleration vector is determined by taking derivative of equation (5) with respect to time:

$$a0 = \begin{bmatrix} 0 \\ 0 \\ 1 \end{bmatrix} \ddot{Z} + \begin{bmatrix} a\ sin\beta \\ 0 \\ a\ cos\beta \end{bmatrix} \ddot{\beta} + \begin{bmatrix} a\ cos\beta \\ 0 \\ -a\ sin\beta \end{bmatrix} \dot{\beta}^2 \tag{6}$$

Figure 3. Forces and torques acting on the QRM[22].

Kinetics of QRM:

Assuming that the model has a linear characteristic [23], the combination of spring damper acting in point B will produce torque T_S

$$T_S = -(T_s^o + c_s\,\beta + d_s\,\dot{\beta}) \tag{7}$$

Where (T_S^0) refers to the pretighting moment (preload in torsional spring), (c_S) refers to spring rate and (d_S) refers to the damping coefficient. The constants (c_x) and (c_z) represents the longitudinal and vertical tire stiffness. By means of hydro pulse effect (actuator), the tire force (F_z) acting in z direction is defined by

$$F_z = -C_z(r_o - r_s) \tag{8}$$

Static tire radius (r_s) (the tire radius under the effect of vehicle load)

$$r_s(t) = a \sin\beta - (u(t) - (h - z + b)) \tag{9}$$

Tire force in x direction (F_x) could be determined from the relation

$$F_x = -C_x(a(1 - \cos\beta) - r_s\varphi) - d_x(a\,sin\beta\dot{\beta} - r_s\dot{\varphi}) \tag{10}$$

Where (F_x) refers to the tire force acting in x direction, (d_x) refers to tire damping in x direction. The torque (T_s) provides the suspension damping that affect riding.

Equations of motion:
According to Jourdan's principle two set of 1st ODE will be result.

$$\dot{y} = Z \qquad q = M.\dot{Z}$$

(11)

For the vector (y) that represents generalized coordinates, the vector (z) represents generalized velocities, Equation (12) represents the mass matrix (M) and Equation (13) represents the vector (q).

$$M = \begin{bmatrix} m_c + m_k + m_w & (sm_k + am_w)cos\beta & 0 \\ (sm_k + am_w)\cos\beta & \theta_k + s^2 m_k + a^2 m_w & 0 \\ 0 & 0 & \theta_w \end{bmatrix}$$

(12)

$$q = \begin{bmatrix} f_z - (m_c + m_k + m_w)g + (sm_k + a\,m_w)sin\beta\dot{\beta}^2 \\ T_s - (s\,m_k + am_w)cos\beta.g + a(f_x sin\beta + f_s cos\beta) \\ -r_s f_x \end{bmatrix}$$

(13)

from the mass matrix, we find that ($m_C + m_K + m_W$) equals the whole masses of QRM and ($\Theta_K + s^2 m_K + a^2\,m_W$) represents the wheel mass inertia, the knuckle, and the trailing arm with respect to the revolute joint in point B. The wheel rotation (φ) is measured with respect to earth-fixed system 0 so the inertia of the wheel (Θ_K) will not present here.

In steady state, the time derivatives of the generalized coordinates will disappear. Then, the suspension torque provided by equation:

$$T_s^{st} = -(T_s^o + C_s \beta^{st})$$

(14)

Tire force in (x and z) directions:

$$f_z^{st} = (m_c + m_k + m_w)g = G$$

(15)

$$f_x^{st} = 0$$

(16)

Trailing arm angle (β_{st}) is represented as follow:

$$a(F_x^{st} \sin\beta_{st} + F_z^{st} \cos\beta_{st}) - (T_s^0 + c_s\beta_{st}) - s_s m_s \cos\beta_{st}\,g = 0$$

(17)

2.2 Modelling results:

From the previous equations of QRM the spring rate (c_s) and the damping ratio (d_s) can be tuned to produce a suitable and tuneable value of the trailing arm angle (β) and the chassis displacement (z).
First , we investigated the changing in the value of initial static angle (β) according to the change in spring rate (c_s) values and the damping ratio (d_s) using matlab.
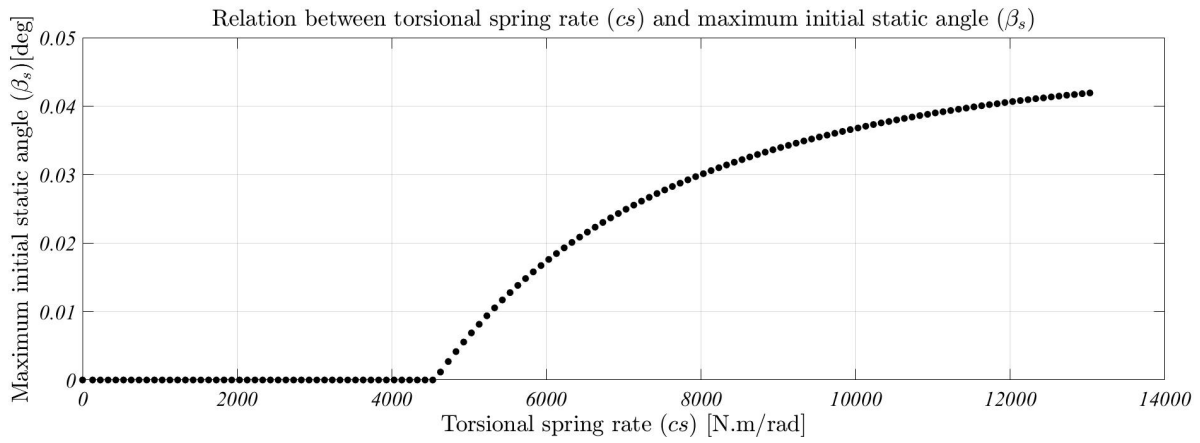
Figure 4. Investigating the angle (β_{st}) by increasing the spring rate (c_S).

It is observed that the angle (β_{st}) doesn't affect by the spring rate value (c_S) until it exceeds the value of ($c_S = 4700$) and after that as the value of spring rate (c_s) increases the angle (β_{st}) increases too.
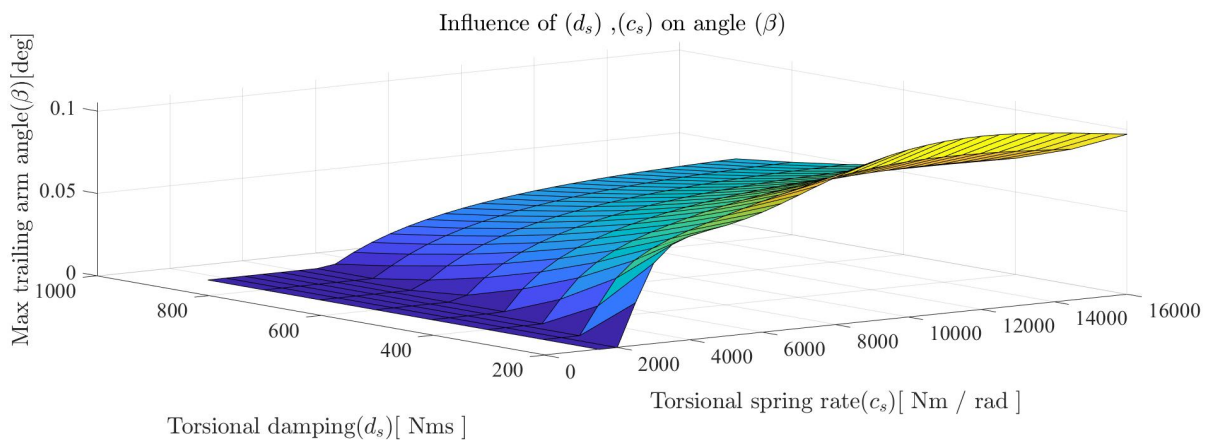
The changing in angle (β_{st}) according to change the value of damping ratio (d_s) can be figured as follow:
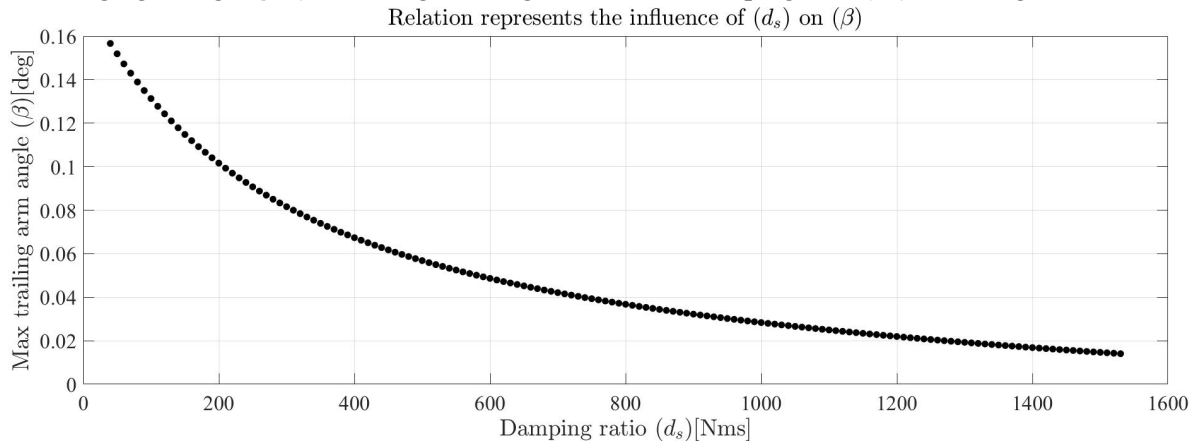
Figure 5. The relation between angle (β_{st}) and the damping ratio (d_s).

It is noticed that the angle (β_{st}) decreases by increasing the damping ratio (d_s) .

The influence of changing the two variables (c_S, d_s) on the angle (β_{st}) can be shown in the next three figures.

**Figure 6.** The influence of changing the two values of (c_S, d_s) on the angle (β_{st}) .
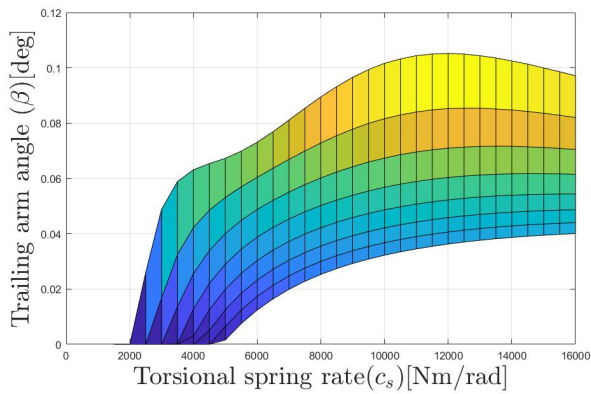
**Figure 7.** (x-z) view shows the influence of spring rate (c_S) on angle (β_{st}).
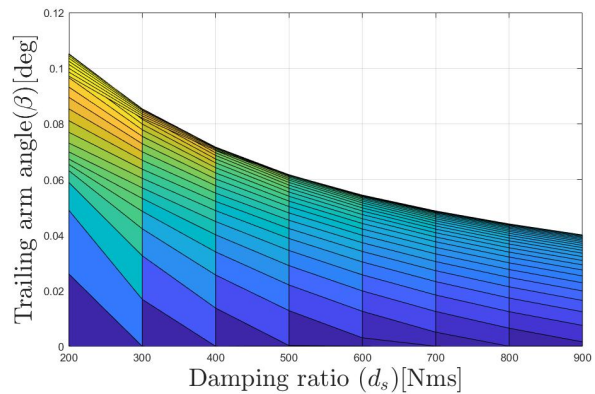
Figure 8. (x-z) view shows the influence of the damping ratio (d_s) on angle (β_{st}).

It is noticed that increasing the spring rate (c_S) works on increasing the angle (β_{st}). Increasing the damping ratio (d_s) works on decreasing the angle (β_{st}).

Second, the change in the value of displacement (z) of the rover body will be investigated according to the change in spring rate (c_s) value using matlab.
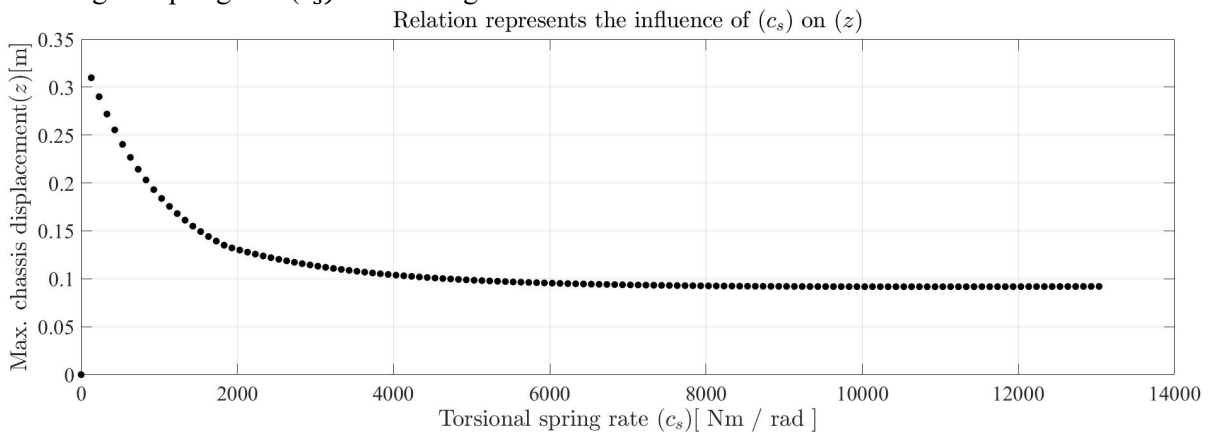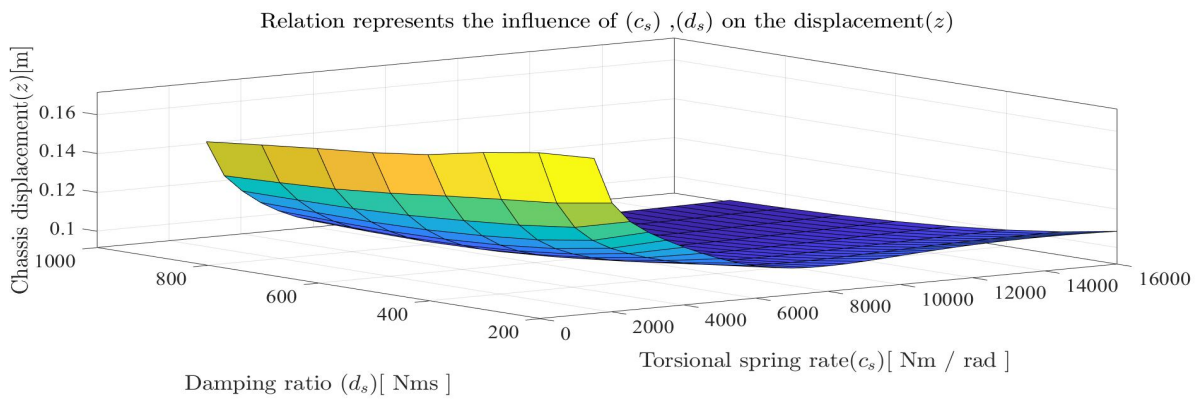

Figure 9. Investigate the displacement (z) of the rover body by increasing spring rate (c_S).

It is noticed that the displacement (z) of the rover body decreases by increasing the value of spring rate (c_S). The rover body displacement (z) change is very small when the spring rate (c_S) value within range (9000:11000), so we can choose spring rate ($c_S = 10000$).
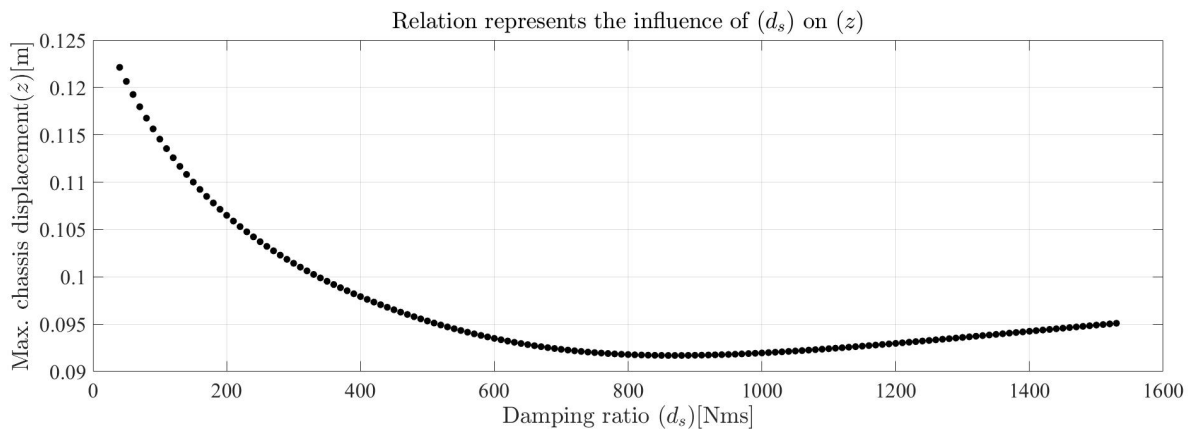

**Figure 10.** Investigate the rover body displacement (z) by increasing the damping ratio (d_s).

It is noticed that the rover body displacement (z) value decreases when the damping ratio value (d_s) increases until it reaches a certain value ($d_s \approx 800\ Nms$) and after that the rover body displacement value starts to increase by increasing the damping ratio value (d_s). The minimum rover body displacement value (z) could be reached when the damping ratio value ($d_s \approx 800$) Nms.

Figure 11. Investigate the displacement (z) of rover body by increasing the damping ratio (d_S) and spring rate (c_S).
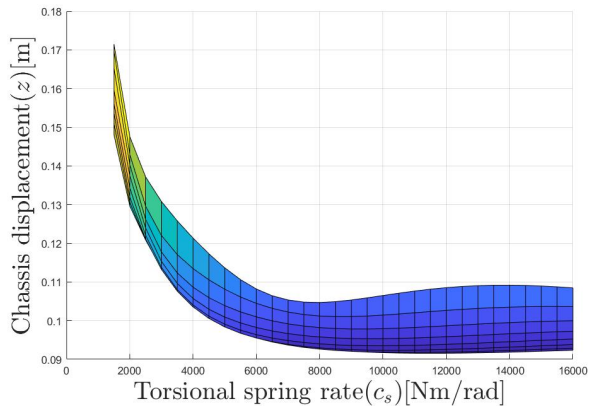
Figure 12. (x-z) view shows the influence of torsional spring rate (c_S) on rover body displacement (z).
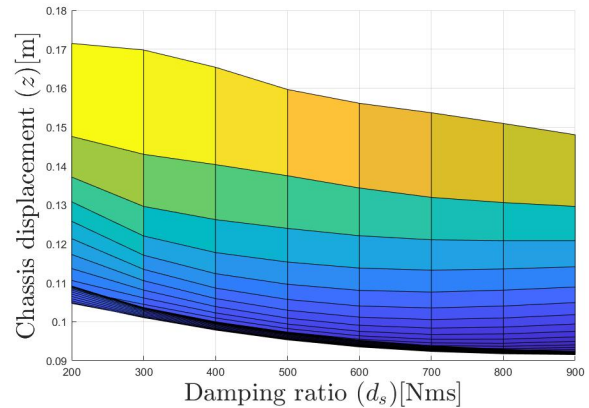
Figure 13. (y-z)view show the influence of damping ratio (d_s) on rover body displacement (z) .

It is noticed that increasing the spring rate(c_S) works on decreasing rover body displacement (z) and increasing the damping ratio (d_s) works on decreasing rover body displacement (z).

3. Road modelling

The road in nature could be irregular due to bumps and obstacles [24]. A rover driving over irregular road or other different terrain will perform pitch, roll and yaw motions. Also if the rover moves on inclination it will induce longitudinal, lateral motions and yawing[25]. Simple road is used to limit the efforts of normal road. So simple road model profile will be used to investigate the influence on QRM.

3.1 Determining of road Profile

The road irregularity with bumps and potholes could be simply represented as a rectangular-shaped and cosine-shaped [26]. The dynamic reaction of QRM according to sudden impact of bump or pothole could be investigated. The bumps and potholes could be simply represents as shown in figure 14.
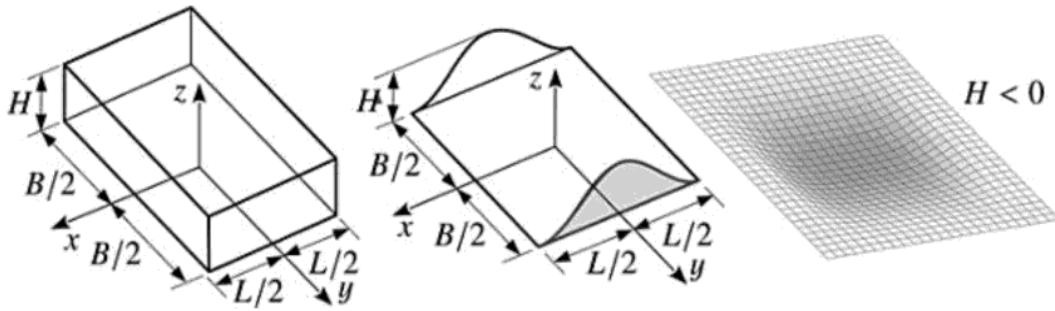
Figure 14. Rectangular and cosine-shaped bump.

The equation represents the rectangular-shaped bump:

$$Z(x,y) = \begin{cases} H & if \\ 0 & else \end{cases} \qquad \frac{-l}{2} < x < \frac{l}{2} \quad \& \quad \frac{-B}{2} < y < \frac{B}{2}$$

(18)

The equation represents the cosine-shaped bump:

$$Z(x,y) = \begin{cases} \frac{1}{2}H & if \\ 0 & else \end{cases} \qquad \frac{-l}{2} < x < \frac{l}{2} \quad \& \quad \frac{-B}{2} < y < \frac{B}{2}$$

(19)

Where H, B, and L represent the height, width, and length of the obstacle.

3.2 Simple road classification

Road profiles can be measured step by step by taking sample points or by using profilometers which is used to measure the surface's profile [27]. The power spectral density (PSD) of simple road outlines shows the drop in magnitude with the number of waves. So that the road irregularity may appear in short distance over the whole distance. So that the PSDs that measured over one meter are nearly some centimetres in amplitude. From the previous explanation the PSD can represent the road outlines as followed.

$$\Phi(\Omega) = \Phi(\Omega_0) \left(\frac{\Omega}{\Omega_0}\right)^{-\omega} \qquad \Omega = \frac{2\pi}{L}$$

(20)

Whereas (Ω) represents the wave number and (Φ_0) represents the value of (PSD) at $(\Omega_0 = 1)$. The waviness (ω) represents the drop in magnitude. According to the standard ISO 8608 (1995)[28], the road profiles could be classified to groups from A to E [29]. For $\omega = 2$, it will be found that each group will have its PSD Φ_0 that is different than the other groups. The waviness that represents the smooth roads (class A) will have $\Phi_0 = 1 * 10^{-6}$, whereas waviness that represents the rough roads (class E) will have $\Phi_0 = 256 * 10^{-6}$.
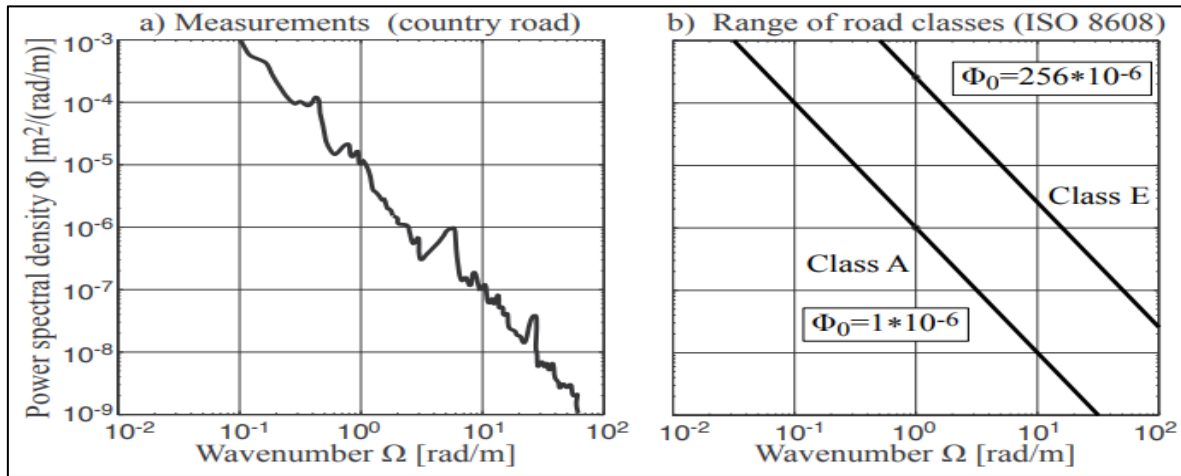
Figure 15. Road PSD: (a) Measured psd, (b) different waviness[2].

Sinusoidal Approximation

A single track can be represented by

$$z_R(s) = \sum_{i=1}^{N} A_i \sin(\Omega_i \, s + \Psi_i) \tag{21}$$

Where $N \rightarrow \infty$

With trailing arm suspension on pseudo random road

$$\Phi(\Omega) = \Phi(\Omega_0)\left(\frac{\Omega}{\Omega_0}\right)^{-\omega} \tag{22}$$

$$A_i = \sqrt{2 \, \Phi(\Omega_i)\Delta\Omega}\,, \qquad i = 1(1)N \tag{23}$$

QRM input on pseudo random road:

$$s \;=\; v\,t \tag{24}$$

$$u = \sum_{i=1}^{N} A_i \sin(\Omega_i \, s + \Psi_i) \tag{25}$$

The amplitudes for pseudo random road

$$A_i = \sqrt{2 \, \Phi(\Omega_i)\Delta\Omega}\,, \qquad i = 1(1)N \tag{26}$$

3.3 Modelling results

According to the previous mathematical equations that describe the road outlines we can obtain the influence of PSD (Φ_0) and the waviness (ω) on the trailing arm angle (β) and the chassis displacement (z_C) using matlab.
First , we will investigate the change in the value of knuckle rotation angle (β) according to the change in PSD (Φ_0) and the waviness (ω) .
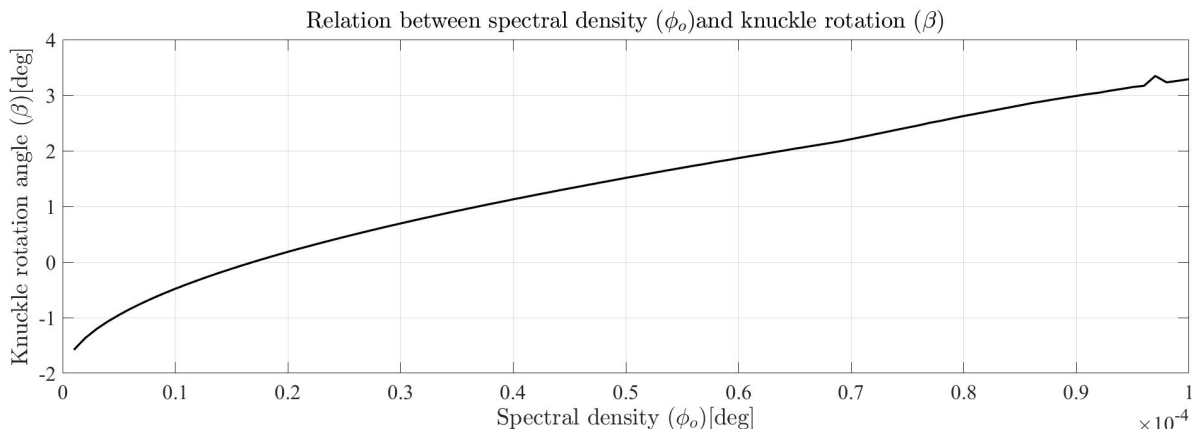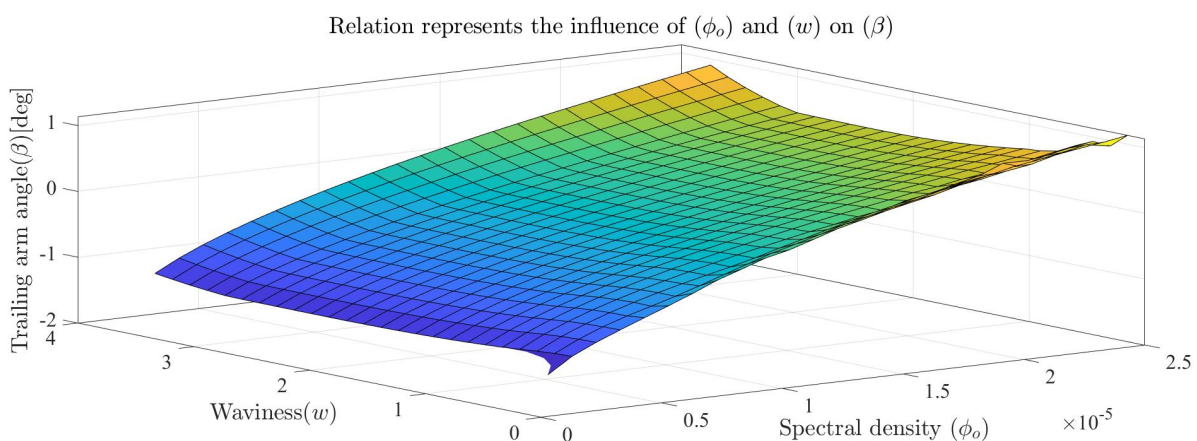
Figure 16. Investigate the trailing arm angle (β) by increasing the PSD (Φ_0).

It is noticed that the trailing arm angle (β) increases by increasing the PSD (Φ_0) according to the previous relations.
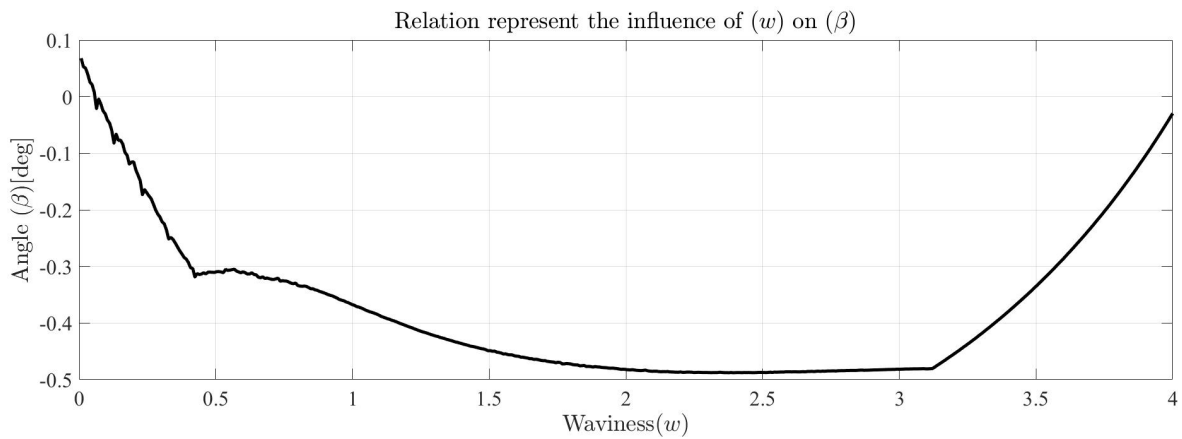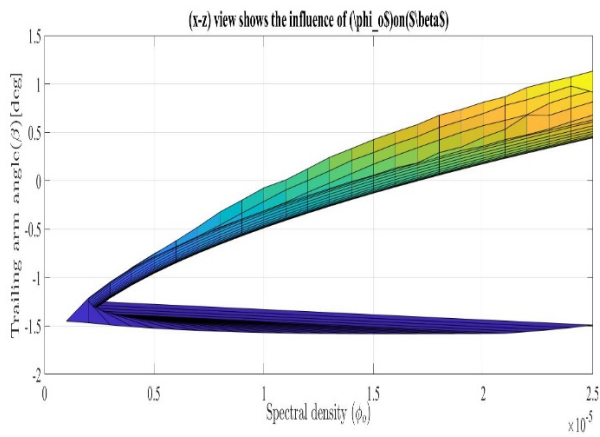

Figure 17. Investigate the static angle (β) by increasing the waviness (ω).
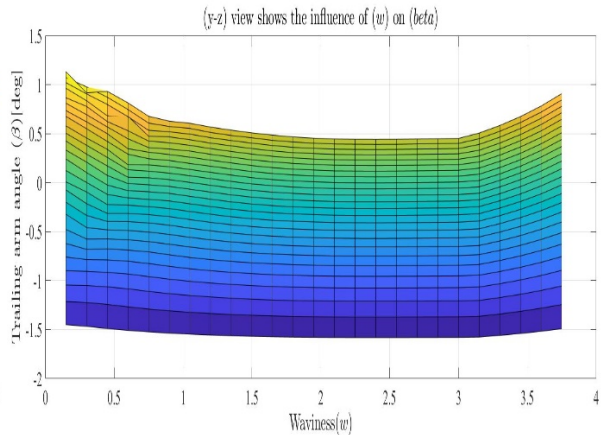
It is noticed that increasing the waviness (ω), the angle (β) decreases until reaching a definite point at ($\omega = 2.4$, $\beta = -0.48712\ deg$) after that the angle (β) increases according to the previous relations.

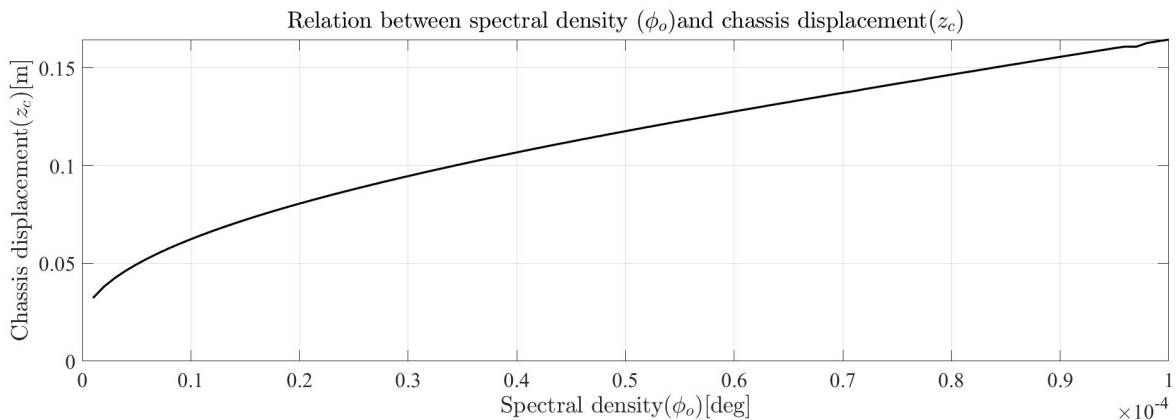**Figure 18.** Investigate the angle (β) by increasing the waviness (ω) and the PSD (Φ_0).

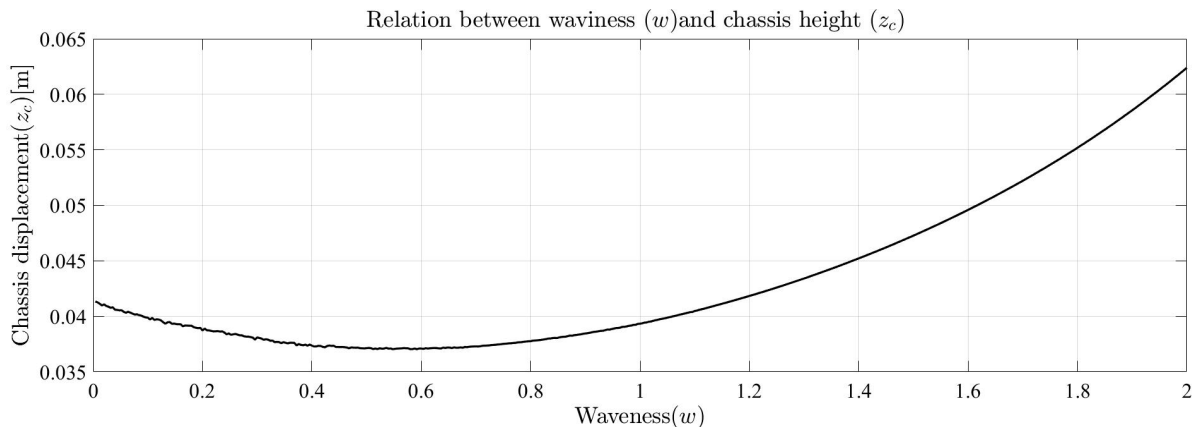**Figure 19.** (x-z) view shows the influence of increasing the PSD (Φ_0) on trailing arm angle (β).

Figure 20. (x-z) view shows the influence of increasing the waviness (ω) on trailing arm angle (β).

It is noticed that increasing the waviness (ω) and Increasing PSD (Φ_0), the angle (β) increases. Decreasing the waviness (ω) and Decreasing PSD (Φ_0), the angle (β) decreases. Increasing the waviness (ω) and Decreasing PSD (Φ_0), the angle (β) decreases. Decreasing the waviness (ω) and Increasing PSD (Φ_0), the angle (β) increases.

Second , we will investigate the change in the value of the chassis displacement (z_C) according to the change in PSD (Φ_0) and the waviness (ω) .
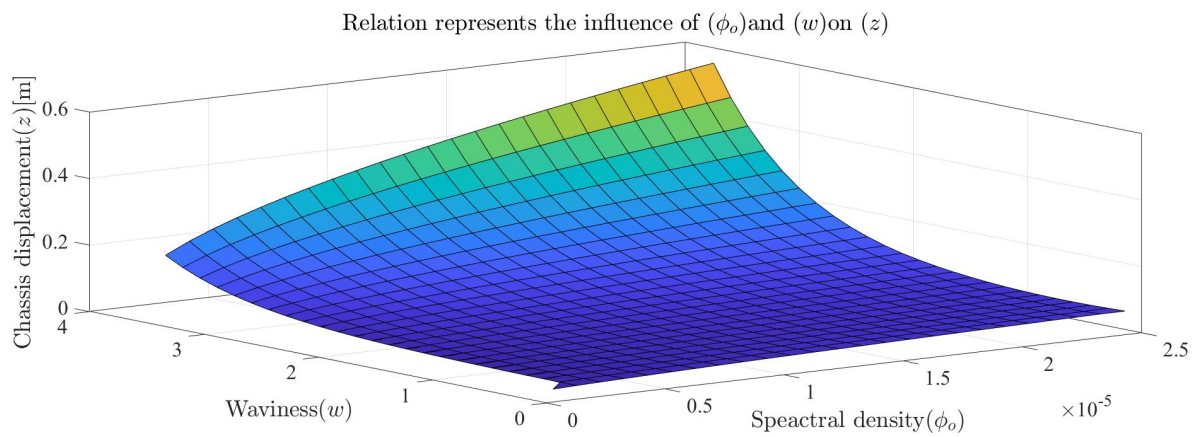

Figure 21. Investigate the displacement (z_C) of the rover body by increasing PSD (Φ_0).

It is noticed that the displacement (z_C) of the rover body increases by increasing PSD (Φ_0), according to the previous relations.
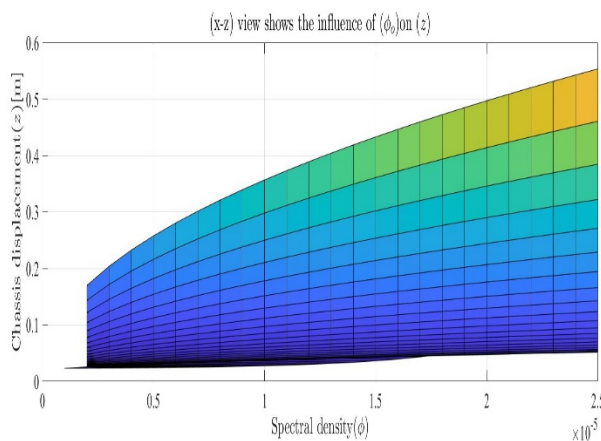
Relation between waviness (w) and chassis height (z_c)

Figure 22. Investigate the displacement (z_C) of the rover body by increasing the waviness (ω).
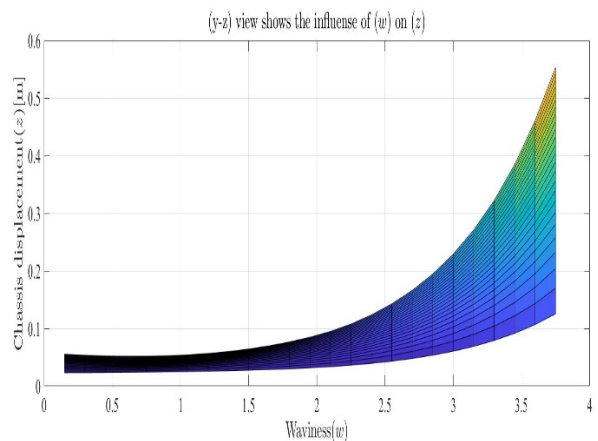
It is noticed that the displacement (z_C) of the rover body increases by increasing the waviness (ω), according to the previous relations.

Relation represents the influence of (ϕ_o) and (w) on (z)

Figure 23. Investigate the displacement (z_C) of the rover body by increasing the waviness (ω) and PSD (Φ_0).

(x-z) view shows the influence of (ϕ_o) on (z)

(y-z) view shows the influence of (w) on (z)

Figure 24. (x-z) view shows the influence of increasing PSD (Φ_0) on the rover body displacement (z_C) .

Figure 25. (y-z) view shows the influence of increasing the waviness (ω) on rover body displacement (z_C).

It is noticed that increasing the waviness (ω) and Increasing PSD (Φ_0), the rover body displacement (z_C) increases. Decreasing the waviness (ω) and Decreasing PSD (Φ_0), the rover body displacement

(z_C) decreases. Increasing the waviness (ω) and Decreasing PSD (Φ_0), the rover body displacement (z_C) increases. Decreasing the waviness (ω) and Increasing PSD (Φ_0), the rover body displacement (z_C) decreases.

4. Conclusion

This paper is divided into two parts .In first part we represent the influence of changing the values of parameters like spring rate (c_S) and damping ratio (d_S) on the trailing arm angle (β) and the rover body displacement (z) ,so that we can obtain a suitable values of (d_S) and (c_S) that result in a required values of (β) and (z) .In the second part we used a model that simulate the road profile aspects to investigate the influence of changing the values of waviness (ω) and PSD (Φ_0), on the trailing arm angle (β) and the rover body displacement (z).

References
[1] Jiregna, I. and G. Sirata, *A review of the vehicle suspension system.* Journal of Mechanical and Energy Engineering, 2020. **4**(2).
[2] Zhang, Q., et al., *Vehicle parameter identification and road roughness estimation using vehicle responses measured in field tests.* Measurement, 2022: p. 111348.
[3] Asfoor, M.S. and A.M. Ali. *Energy-efficient electrification of public transportation fleets based on generic driving cycles for the city of Cairo, Egypt.* in *2021 IEEE Vehicle Power and Propulsion Conference (VPPC).* 2021. IEEE.
[4] M. Ali, A. and D. Söffker. *Realtime application of progressive optimal search and adaptive dynamic programming in multi-source HEVs.* in *Dynamic Systems and Control Conference.* 2017. American Society of Mechanical Engineers.
[5] Ali, A.M. and M.I. Yacoub. *Optimal predictive power management strategy for fuel cell electric vehicles using neural networks in real-time.* in *2020 IEEE Vehicle Power and Propulsion Conference (VPPC).* 2020. IEEE.
[6] M. Ali, A. and D. Söffker. *Realtime power management of a multi-source HEV using adaptive dynamic programing and probabilistic drive state model.* in *International Design Engineering Technical Conferences and Computers and Information in Engineering Conference.* 2017. American Society of Mechanical Engineers.
[7] Ali, A.M. and M.S. Asfoor, *Optimal Battery Sizing and Stops Allocation for Electrified Fleets Using Data-Driven Driving Cycles: A Case Study for the City of Cairo.* IEEE Transactions on Transportation Electrification, 2022.
[8] Becker, C.M. and P.S. Els, *Profiling of rough terrain.* International Journal of Vehicle Design, 2014. **64**(2-4): p. 240-261.
[9] Naoumov, V.I., et al. *Experience of the Incorporation of NASA Human Exploration Rover Challenge Program in the Mechanical Engineering Curriculum.* in *AIAA Scitech 2019 Forum.* 2019.
[10] Ali, A.M., R. Shivapurkar, and D. Soeffker. *Development and improvement of a situation-based power management method for multi-source electric vehicles.* in *2018 IEEE Vehicle Power and Propulsion Conference (VPPC).* 2018. IEEE.
[11] Hurel, J., A. Mandow, and A. García-Cerezo, *Kinematic and dynamic analysis of the McPherson suspension with a planar quarter-car model.* Vehicle System Dynamics, 2013. **51**(9): p. 1422-1437.
[12] Ipakchian Askari, S., A. Haans, and W.A. IJsselsteijn, *Uncovering terra incognita in the AHD design space: A review of affective haptic devices.* Frontiers in Computer Science, 2022. **4**.
[13] Kruczek, A. and A. Stribrsky. *A full-car model for active suspension-some practical aspects.* in *Proceedings of the IEEE International Conference on Mechatronics, 2004. ICM'04.* 2004. IEEE.
[14] Giua, A., C. Seatzu, and G. Usai, *A mixed suspension system for a half-car vehicle model.* Dynamics and Control, 2000. **10**(4): p. 375-397.

[15] Taffo, G.K., M.S. Siewe, and C. Tchawoua, *Stability switches and bifurcation in a two-degrees-of-freedom nonlinear quarter-car with small time-delayed feedback control.* Chaos, Solitons & Fractals, 2016. **87**: p. 226-239.

[16] Singh, W.S. and N. Srilatha, *Design and analysis of shock absorber: a review.* Materials Today: Proceedings, 2018. **5**(2): p. 4832-4837.

[17] Ali, A.M., R. Shivapurkar, and D. Söffker, *Optimal situation-based power management and application to state predictive models for multi-source electric vehicles.* IEEE Transactions on Vehicular Technology, 2019. **68**(12): p. 11473-11482.

[18] Shirahatti, A., et al., *Optimal design of passenger car suspension for ride and road holding.* Journal of the Brazilian Society of Mechanical Sciences and Engineering, 2008. **30**: p. 66-76.

[19] Naudé, A. and J. Snyman, *Optimisation of road vehicle passive suspension systems. Part 1. Optimisation algorithm and vehicle model.* Applied Mathematical Modelling, 2003. **27**(4): p. 249-261.

[20] Koch, G., et al., *Design and modeling of a quarter-vehicle test rig for active suspension control.* 2010, Lehrstuhl für Regelungstechnik.

[21] Rónai, L., *Investigation of the Vibrational Behavior of a Quarter-Car Model*, in *Vehicle and Automotive Engineering 4: Select Proceedings of the 4th VAE2022, Miskolc, Hungary.* 2022, Springer. p. 824-834.

[22] Rill, G., *Road vehicle dynamics: fundamentals and modeling.* 2011: Crc Press.

[23] Maher, D. and P. Young, *An insight into linear quarter car model accuracy.* Vehicle system dynamics, 2011. **49**(3): p. 463-480.

[24] Rouillard, V., M.A. Sek, and B. Bruscella, *Simulation of road surface profiles.* Journal of transportation engineering, 2001. **127**(3): p. 247-253.

[25] Ali, A.M. and B. Moulik, *On the role of intelligent power management strategies for electrified vehicles: A review of predictive and cognitive methods.* IEEE Transactions on Transportation Electrification, 2021. **8**(1): p. 368-383.

[26] Varona, B., A. Monteserin, and A. Teyseyre, *A deep learning approach to automatic road surface monitoring and pothole detection.* Personal and Ubiquitous Computing, 2020. **24**(4): p. 519-534.

[27] Spangler, E.B. and W.J. Kelly, *GMR road profilometer-a method for measuring road profile.* Highway Research Record, 1965. **121**: p. 27-54.

[28] Múčka, P., *Passenger Car Vibration Dose Value Prediction Based on ISO 8608 Road Surface Profiles.* SAE International Journal of Vehicle Dynamics, Stability, and NVH, 2021. **5**(10-05-04-0029): p. 425-441.

[29] Dodds, C. and J. Robson, *The description of road surface roughness.* Journal of sound and vibration, 1973. **31**(2): p. 175-183.